IEEE Access
Multidisciplinary | Rapid Review | Open Access Journal

Received February 24, 2019, accepted March 20, 2019, date of publication April 1, 2019, date of current version April 13, 2019.

Digital Object Identifier 10.1109/ACCESS.2019.2908395

INVITED PAPER

Design and Analysis of a Graphene Magneto-Plasmon Waveguide for Plasmonic Mode Switch

MOHSEN HEIDARI, (Student Member, IEEE), AND VAHID AHMADI, (Senior Member, IEEE)
Department of Electrical and Computer Engineering, Tarbiat Modares University, Tehran 14115111, Iran

Corresponding authors: Mohsen Heidari (mh.heidari@modares.ac.ir) and Vahid Ahmadi (v_ahmadi@modares.ac.ir)

This work was supported by the Tarbiat Modares University under Grant #IG-39703.

ABSTRACT In this paper, we design and investigate a graphene magneto-Plasmon waveguide for plasmonic mode switch application. First, an analytical model based on effective index method is presented to extract waveguide properties, such as effective index, effective guide width, cutoff wavelength, and the number of guided modes. We then verify the results with the finite element method. Due to the strong magneto-optical activity of graphene under an external magnetic field, waveguide properties can be widely tuned magnetically. Here, using a combination of several parameters, including chemical potential, magnetic field, and structure width, we manipulate the waveguide properties, such as mode confinement and the number of guided modes in order to achieve desired functions. The results demonstrate that the proposed structure acts as a mode switch device. Namely, for a given chemical potential and wavelength, the guided modes are controlled by the magnetic field. Moreover, we show that the waveguide becomes non-reciprocal in the presence of a magnetic field, which enables the structure to act as a plasmonic isolator and circulator.

INDEX TERMS Dielectric-loaded waveguide, graphene, isolators, magneto-optic devices, optical switch, nonreciprocal devices, surface magneto-plasmons, unidirectional components.

I. INTRODUCTION

Surface plasmons (SPs) which are electromagnetic surface waves propagating on a dielectric-metal interface originate from the interaction of free electrons and electromagnetic fields [1], [2]. Due to high confining property that could break diffraction limit, plasmonic devices offer a promising road to realizing ultra-compact photonic circuits [3]–[5]. In the visible to the near-infrared ranges of spectrum noble metals in conjunction with dielectric media usually are used for supporting SPs. SP fields strongly are confined to the metal-dielectric interface, are very sensitive to refractive index variation can be used for active control of SPs. However, due to the week refractive index changes of noble metals, active control of SPs requires active dielectric media [6], [7]. Depending on the active dielectric properties, several mechanisms such as thermo- [7], electro- [8] and magneto-optic [9] effects can be employed to control SPs. In the terahertz (THz) and mid-infrared regions of the spectrum, poor confinement and the relatively high propagation loss of metal-dielectric plasmons, make noble metal less applicable [10]. These challenges can be solved by graphene. Graphene has unique properties, such as gate tunability [11], quantum Hall effect [12], the capability of supporting both transverse magnetic (TM) and transverse electric (TE) SPs modes [13]. Moreover, compared with metal-dielectric SPs, graphene SPs have a much smaller wavelength, and lower propagation loss than that of metals in the mid-infrared and THz spectral region [14]–[17]. Because of such capabilities, increasing attention has been paid to graphene for realizing active plasmonic and magneto-plasmonic devices [2], [18]–[20].

Magneto-optical (MO) devices such as isolators, circulators, and polarization rotators are the key components of photonic circuits [21]–[23]. MO materials due to their unique properties, for example, the breaking of the time-reversal symmetry of the interacting electromagnetic wave leads to the emergence of nonreciprocal phenomena such as Faraday rotation, MO Kerr effect, and nonreciprocal phase shift [24]. Conventional MO photonic devices based on bulk MO materials suffer from weak MO activity, leading to

The associate editor coordinating the review of this manuscript and approving it for publication was Sukhdev Roy.

large-scale footprints at least several tens of wavelength (tens of micrometers), thereby challenging the implementation of highly integrated photonic circuits [19], [24]. Thus, there is an increasing demand for miniaturizing these devices for future generation of integrated photonic technology. The realization of integrated nanoplasmonic circuitry, a plasmonic analogy to nonreciprocal photonic devices are needed. Therefore, MO material and devices need to be shrunk to nanoplasmonic regime.

Magneto-plasmonic circuits can be realized by following configurations, either a ferromagnetic metal in contact with a dielectric medium [25] or a noble metal with a ferromagnetic dielectric [24]. However, ferromagnetic metals such as Ni, Co, and Fe are too lossy [26] to be employed in plasmonic structures. On the other hand, one of the significant challenges in magneto-plasmonic devices based on the MO dielectric materials like garnets is an inherent limitation to integrate into photonic platforms, such as silicon complementary metal-oxide-semiconductor (CMOS) and III-V semiconductor fabrication technology [26]. This restriction is due to the lattice mismatch between garnets and the substrate [27], and also the requirement of thermal annealing. Furthermore, the fabrication of garnet-based devices needs a hybrid integration technique like wafer bonding or a deposition technique (e.g., pulsed laser deposition) [28].

The strong MO activity of graphene combined with the capability of supporting deep-subwavelength SPs and wide-range tuning of SPs makes graphene as a potential candidate for ultra-compact active plasmonic and nonreciprocal [21]–[23]. Moreover, the unique properties of graphene such as small device footprint, compatibility with CMOS and other fabrication technologies, the versatility, ultra-wideband, and the high-speed operation make graphene an attractive option [29]. Previously, the MO effect in infinite graphene sheet [2], graphene-coated nanowire [30], graphene-dielectric sandwich [20] was studied. Also, the nonreciprocity of the edge surface magneto-plasmons (SMPs) of graphene microstrip has been studied [31]. In [32], dielectric-loaded graphene surface plasmon waveguide has been proposed and propagating properties in the absence of the magnetic field and, their tunability (by changing Fermi energy level) has been demonstrated. Compared with graphene microribbon waveguides, dielectric loaded graphene magneto-plasmon waveguides (DLGMPW) shows better immunity to production tolerances and can be easily fabricated using current lithography technology.

Moreover, the employment of magnetic field to the dielectric loaded structures, not only provides more freedom to manipulate SPs but also gives the opportunity to design novel nonreciprocal devices such as on-chip circulators, isolators, phase shifters and couplers [31], [33], [34]. Therefore, it is of great necessity to investigate the properties of SMP modes in DLGMPW. Nevertheless, the propagating characteristics of SMPs and the capability of extreme-tunability via an external magnetic field, and their influences on nonreciprocity has not been studied yet in dielectric-loaded waveguides.

In this paper, for the first time, we study the SMP modes propagating in a DLGMPW in terahertz regime under an external magnetic field. We present an analytical model based on effective index method (EIM) to calculate the Eigen modes of the structure. The accuracy of the analytical results is confirmed by finite element calculation. Then, mode dispersion and propagation characteristics of DLGMPW and single-mode operation condition are investigated. After that, the tunable characteristics of DLGMPW-based devices are scrutinized by the proposed analytical model. The chemical potential, magnetic field strength, and dielectric strip width are explored to provide the guidelines for designing novel plasmonic devices with new functionalities such as plasmonic mode switch, and ultrasensitive sensor. Finally, the nonreciprocal properties of DLGMPW are discussed, which can be employed for realizing plasmonic isolators, circulators, and unidirectional components.

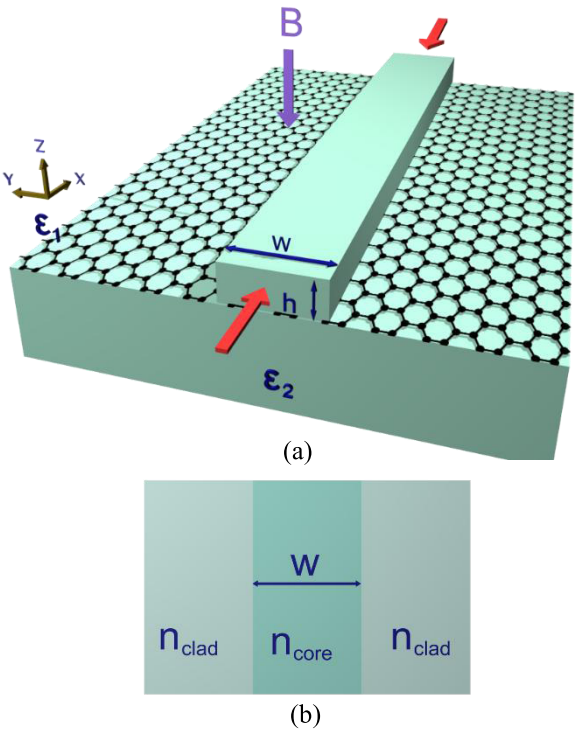

FIGURE 1. (a) Schematic of dielectric-loaded graphene magneto-plasmon waveguide. (b) The equivalent three-section dielectric planar waveguide based on EIM.

II. ANALYTICAL MODEL AND FEM VERIFICATIONS

The schematic view of a DLGMPW is shown in Fig. 1(a). We consider a graphene layer placed at the interface of two dielectric media: the substrate with relative permittivity of ε_1 and the dielectric strip with a relative permittivity of ε_2. The dielectric strip width and height are w and h, respectively. The dielectric strip on the top of graphene leads to a higher refractive index for SMPs modes on the dielectric-graphene-dielectric interface compared to that of the air-graphene-dielectric interface.

The EIM is one of the efficient methods widely applied in sophisticated photonic and plasmonic structures [32], [35], [36]. Here, we use EIM to analyze and derive an analytical model to analyze DLGMPW. In this method, DLGMPW reduces to a three-section dielectric planar waveguide, as clad/core/clad, as shown in Fig. 1(b). The refractive indices of the core and the clad regions, n_{core} and n_{clad}, are equal to the effective mode index of SMPs in each region and are written as:

$$n_{\text{core}} = \beta_{\text{SMP}_{\text{core}}}/k_0 \tag{1a}$$
$$n_{\text{clad}} = \beta_{\text{SMP}_{\text{clad}}}/k_0 \tag{1b}$$

where $\beta_{\text{SMP}_{\text{core}}}$ and $\beta_{\text{SMP}_{\text{clad}}}$ are the wave vector of SMP in the core and clad regions respectively, and k_0 is the vacuum wave number. Due to an external magnetic field, the surface conductivity of graphene, σ becomes anisotropic tensor as [21]:

$$\sigma = \begin{pmatrix} \sigma_{xx} & \sigma_{xy} \\ \sigma_{yx} & \sigma_{yy} \end{pmatrix} \tag{2}$$

where $\sigma_{xx} = \sigma_{yy}$ and σ_{xy}=-σ_{yx} are the longitudinal and Hall components of conductivity, respectively. By inclusion of quantum response of graphene, they are written as [37], [38]:

$$\sigma_{xx} = \frac{e^2 v_F^2 |eB| \hbar(\omega - j2\Gamma)}{-j\pi} \times \sum_{n=0}^{\infty} \left\{ \begin{array}{l} \frac{1}{M_{n+1}-M_n} \times \frac{f(M_n)-f(M_{n+1})+f(-M_{n+1})-f(-M_n)}{(M_{n+1}-M_n)^2-\hbar^2(\omega-j2\Gamma)^2} \\ +(M_n \to -M_n) \end{array} \right\} \tag{3}$$

$$\sigma_{xy} = -\frac{e^2 v_F^2 |eB|}{-\pi} \times \sum_{n=0}^{\infty} \left\{ \begin{array}{l} \frac{1}{M_{n+1}-M_n} \times \frac{f(M_n)-f(M_{n+1})+f(-M_{n+1})-f(-M_n)}{(M_{n+1}-M_n)^2-\hbar^2(\omega-j2\Gamma)^2} \\ +(M_n \to -M_n) \end{array} \right\} \tag{4}$$

where $M_n = \sqrt{2n|eB|\hbar v_F^2}$ denotes Landau level energy with the index n and $f = \frac{1}{\exp(E-\frac{\mu}{kbT})+1}$ is Fermi-Dirac distribution. In (3) and (4), c, e, $\hbar$, and v_F are light velocity in vacuum, electron charge, reduced Planck's constant and Fermi velocity in graphene, respectively. Also, B, Γ, μ, and T represent applied external magnetic flux density perpendicular to the graphene sheet, scattering rate, chemical potential, and temperature, respectively.

To determine $\beta_{\text{SMP}_{\text{core}}}$ and $\beta_{\text{SMP}_{\text{clad}}}$, the dispersion relations of SMPs in the core and the clad regions are obtained with the following electromagnetic boundary conditions at the interface, z=0:

$$z \times (\vec{E_2} - \vec{E_1})\Big|_{z=0} = 0 \tag{5a}$$
$$z \times (\vec{H_2} - \vec{H_1})\Big|_{z=0} = \vec{J} \tag{5b}$$

For 2D graphene sheet, with a frequency dependent 2×2 conductivity tensor $\overline{\sigma}$ as expressed in (2), we have $\vec{J} = \overline{\sigma}\vec{E}_t$, where $\vec{J}$ is surface current density, and $\vec{E_t}$ is the tangential component of the electric field.

Equations (5a) and (5b) lead to the continuity of the tangential component of the electric field and discontinuity of the tangential component of the magnetic field, which yields:

$$\vec{E}_{1t} = \vec{E}_{2t} \tag{6a}$$
$$\vec{H}_{1y} - \vec{H}_{2y} = -\sigma_{xx}\vec{E}_{1x} - \sigma_{xy}\vec{E}_{1y} \tag{6b}$$
$$\vec{H}_{1x} - \vec{H}_{2x} = -\sigma_{xy}\vec{E}_{1y} + \sigma_{xx}\vec{E}_{1x} \tag{6c}$$

It is straightforward to combine the above results and obtain SMPs dispersion relation as:

$$[\frac{j\omega\epsilon_0\epsilon_1}{\kappa_1} + \frac{j\omega\epsilon_0\epsilon_2}{\kappa_2} - \sigma_{xx}] \times [\frac{\kappa_1}{j\omega\mu_0\mu_1} + \frac{\kappa_2}{j\omega\mu_0\mu_2} - \sigma_{xx}] = -\sigma_{xy}^2 \tag{7}$$

The dispersion relation is in excellent agreement with the reported results in [2], [39]. In (7), ϵ_0 and μ_0 are the vacuum permittivity and permeability, ϵ_1, ϵ_2, and μ_2 are relative permittivity, and permeability in two dielectric media. Here, $\kappa_1 = \sqrt{\beta^2 - \frac{\omega^2\epsilon_1\mu_1}{c^2}}$, $\kappa_2 = \sqrt{\beta^2 - \frac{\omega^2\epsilon_2\mu_2}{c^2}}$, and β is propagation constant. Now, by solving (7) in the core and cladding region, $\beta_{\text{SMP}_{\text{core}}}$ and $\beta_{\text{SMP}_{\text{clad}}}$, and, therefore n_{core} and n_{clad} are determined.

As shown in Fig. 1 (b), we use the EIM to model DLGMPW as a three-layer dielectric slab waveguide, which is a simple, intuitive idea on the mode propagation characteristics. Moreover, this model yields accurate results and is fast to execute. It is well-known that such dielectric slab waveguides, satisfy the following condition [40], [41]:

$$\xi w = m\pi + 2\Phi \quad m = 0, 1, 2, \ldots \tag{8}$$

Here, m is the mode number, $\Phi = \tan^{-1}(\frac{n_{\text{core}}^2\gamma_c}{n_{\text{core}}^2\xi})$, $\gamma_c = k_0\sqrt{n_{\text{eff}}^2 - n_{\text{clad}}^2}$, and n_{eff} is the effective index of the m-th order guided mode. After simple algebraic manipulation, the eigenmode equation for the m-th order guided mode is derived as:

$$(\frac{n_{\text{clad}}^2}{n_{\text{core}}^2})\xi \tan(\frac{\xi w - m\pi}{2}) = \gamma_c \tag{9}$$

This equation can be solved numerically for each m-th order mode individually, and n_{eff} is derived.

Now, we study characteristics of such waveguides including the effective guided width and cutoff wavelength. It is noteworthy that the whole field of any guided mode, are not confined in the core region. Always a portion of the guided mode propagates through the clad region. As the wavelength increases, the power portion, which penetrates in the clad region, grows up. So we introduce the effective guide width, w_{eff}, that is a measure for the region in which the guided SMPs concentrate and propagate. The effective width, which is derived based on the procedure reported in [40], [41] is defined as:

$$w_{\text{eff}} = w + \frac{2}{(\frac{n_{\text{eff}}^2}{n_{\text{core}}^2} + \frac{n_{\text{eff}}^2}{n_{\text{clad}}^2} - 1)\gamma_c} \tag{10}$$

When the wavelength approaches the cutoff, a significant portion of field spreads over the clad region. At the cutoff condition, $\frac{n_{\text{eff}}}{n_{\text{clad}}} \approx 1$, no bounded mode in the core can propagate. By substituting $n_{\text{eff}} = n_{\text{clad}}$ in (9), the cutoff wavelength of m-th order guided mode is obtained as [32]:

$$\lambda_{\text{cm}} = \frac{2w}{m}\sqrt{\text{Re}(n_{\text{core}}^2) - \text{Re}(n_{\text{clad}}^2)} \tag{11}$$

In (11), m=1 corresponds to the single mode operation, which is of the most important to obtain desired behavior in many applications [32], [42].

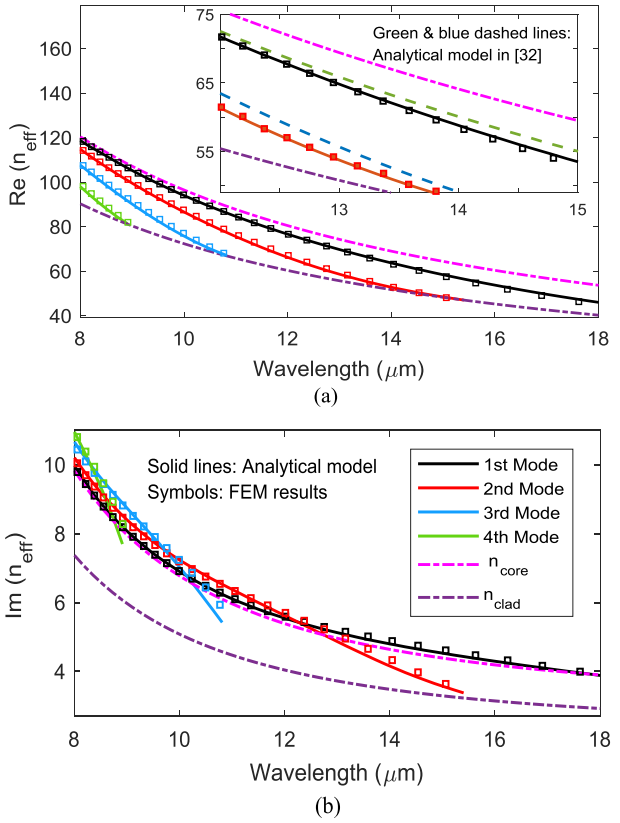

FIGURE 2. Effective indices of SMP modes in DLGMPW with a width of 200 nm for case (i) without magnetic field: (a) Real part, (b) Imaginary part of effective mode index. The inset of (a) shows the comparison of our analytical model (black and blue solid lines), FEM results (black and red symbols) and the model proposed in [32] (dark green and dark blue dashed lines) for the first and the second order modes.

III. RESULTS AND DISCUSSIONS

At first, we solve the SMP's dispersion relation expressed by (8) to obtain n_{core} and n_{clad} needed in the proposed EIM-based analytical model for the m-th order guided mode of DLGMPW. To validate the proposed analytical model, we compare the results with FEM simulation using commercial software (COMSOL Multiphysics). Comparing our analytical model to that proposed in [32], we show that our model has better accuracy. Next, the single-mode and multimode operation ranges of DLGMPW are calculated for different parameters, such as strip's width, w, and the external magnetic flux density, B. In our calculations, we assume the relative permittivity of the dielectric strip and the substrate to be 1.96, and the height of the dielectric strip, h is 100 nm.

The real and imaginary parts of the effective index of SMPs in DLGMPW with a width of 200nm are investigated for two cases: (i) without magnetic field; (ii) with an external magnetic field of 1 T. Figs 2 (a) and (b) show the real and imaginary parts of the effective index in the absence of the magnetic field. Both the real and imaginary parts of the effective index of the SMPs decrease as the wavelength increases. As depicted in Fig. 2 (a) and 2(b), the fundamental mode with the highest effective index, is cutoff free (its cutoff wavelength extends to the longer wavelengths, not depicted in this range), however the cutoff wavelengths of the other modes occur at the point where their effective indices approach n_{clad}. The 2$^{\text{nd}}$, 3$^{\text{rd}}$, and the 4$^{\text{th}}$ modes reach to the cutoff at the wavelengths of 15.1μm, 10.91μm, and 8.87μm, respectively. We can observe that our analytical model is in excellent agreement with FEM simulation results over the entire wavelength range, even near the cutoff wavelength (see the inset of Fig. 2(a)).

Figs. 3 (a) and (b) show the real and imaginary parts of the effective index in the presence of the magnetic field. Same as the case (i), in case (ii), the real and imaginary parts of the effective index decrease as the wavelength increases. However, due to the magnetically-induced optical resonances associated with transitions between Landau-levels, the imag-

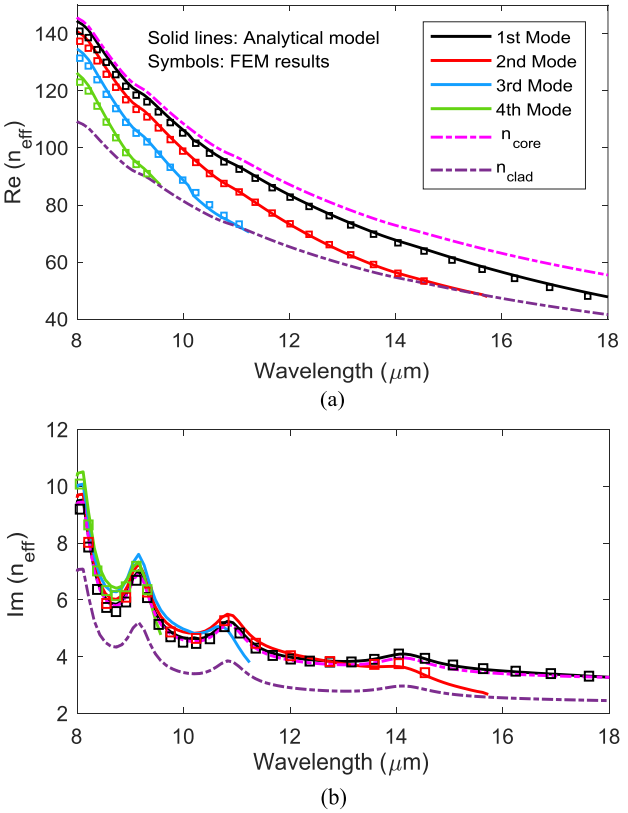

FIGURE 3. Effective indices of SMP modes in DLGMPW with a width of 200 nm for case (ii) with an external magnetic field of B=1 T: (a) Real part, (b) Imaginary part of effective mode index.

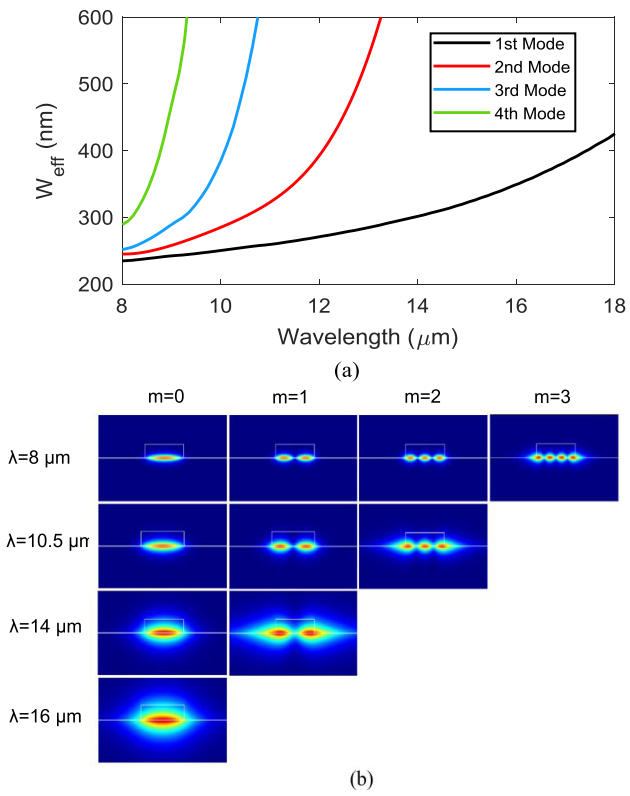

FIGURE 4. (a) The effective guide width of the four lowest order modes of DLGMPW. (b) mode patterns of the first four order modes at different wavelengths of 8 μm, 10.5 μm, 14 μm, and 16 μm.

inary part does not vary uniformly and shows several peaks. Moreover, the mode confinement decreases as a function of wavelength. According to the results of Fig. 3(a) and (b), the 2nd, 3rd, and the 4th modes reach cutoff at the wavelengths 15.72 μm, 11.24 μm, and 9.57 μm, respectively. Compared to Figs. 2(a) and 2(b), in the presence of a magnetic field, cutoff wavelengths are red shifted. Also, both real and imaginary parts of the effective index decrease inversely with wavelength. Moreover, the mode confinement decreases as a function of wavelength. Therefore, the guided mode area becomes larger and spreads into the clad regions.

The effective guide widths, w_{eff}, of DLGMPW are shown in Fig. 4(a) for the first four modes. The effective widths of all modes increase as a function of wavelength and for the higher order modes (m=1,2,3), and a sharp increment is observed compared to that of the fundamental mode (m=0). It is important to note that, for all modes, when the wavelength approaches the cutoff point, the modes are not bounded to the core region, and extends to the clad region as well (see Fig. 4(b)). For instance, at $\lambda = 8\mu$m we have four modes, however by increasing the wavelength to 10.5μm, 14μm and 16μm the effective guide thickness increases, so we have three, two and one modes, respectively.

Single-mode operation condition can be obtained, if the strip width is small enough. Single-mode and multimode operation region of DLGMPW are determined by solving (11). Fig. 5 shows single-mode and multimode operation regions as a function of wavelength and strip width, for different magnetic flux densities of $B = 0,3,5$ T in Figs. 5(a), 5(b), and 5(c), respectively. For all the cases the chemical potential is assumed to be $\mu = 0.175$ eV. The regions are labeled by 1,2,3,4 which corresponds to the number of guided modes. The operation region of each number of modes is separated by a boundary dashed line (cutoff wavelength line) from the other region. The single-mode

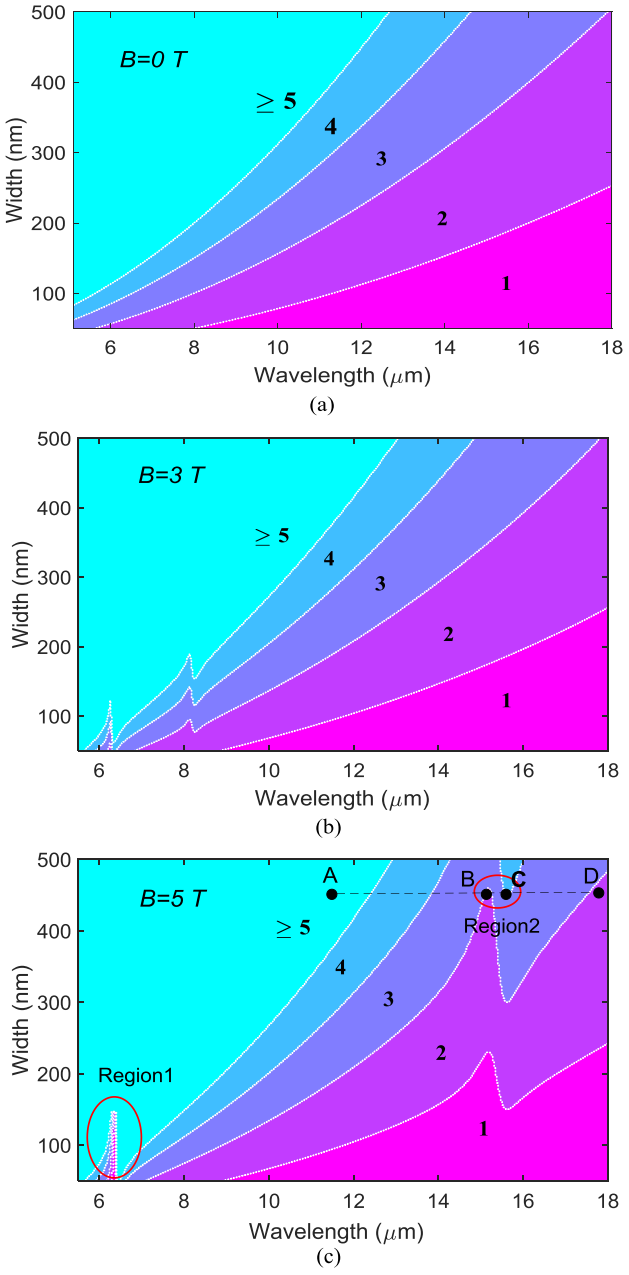

FIGURE 5. Single-mode and multimode operation region of DLGMPW as a function of wavelength and strip width, for different values of the magnetic field. The chemical potential is $\mu = 0.175$ eV and the number of guided modes are labeled on each region. (a) zero magnetic field. (b) B=3 T. (c) B=5 T. The dashed white curves show the cutoff lines of higher order modes.

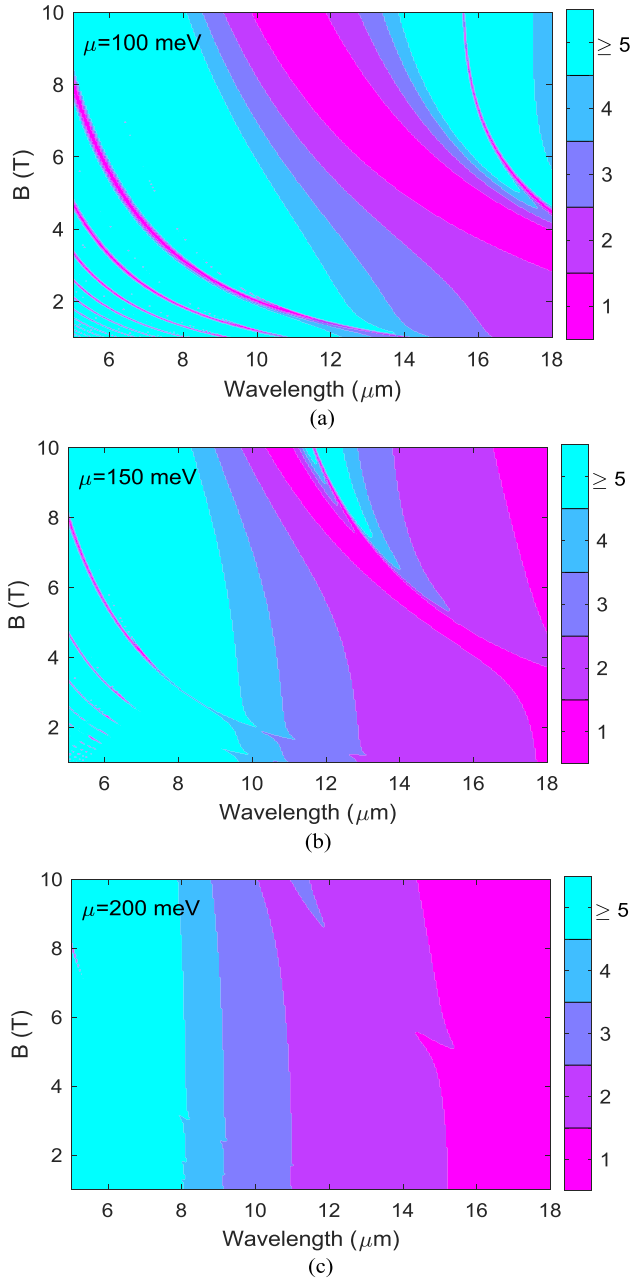

FIGURE 6. Single-mode and multimode operation region of DLGMPW as a function of wavelength and magnetic field at different values of chemical potential. The strip width is w=200 nm. The number of guided modes are specified by different colors as shown in the color bar.

operation region labeled by 1, is located at the bottom of the first order mode (m=1) cutoff wavelength line. At each wavelength, when the strip width reduces to a critical value, the single-mode condition is satisfied. It can be seen that the magnetic field dramatically changes the boundaries of single-mode/multimode operation regions (dashed lines in the Figs.). The starting point of the single mode operation region is shifted to the longer wavelength as the magnetic field increases.

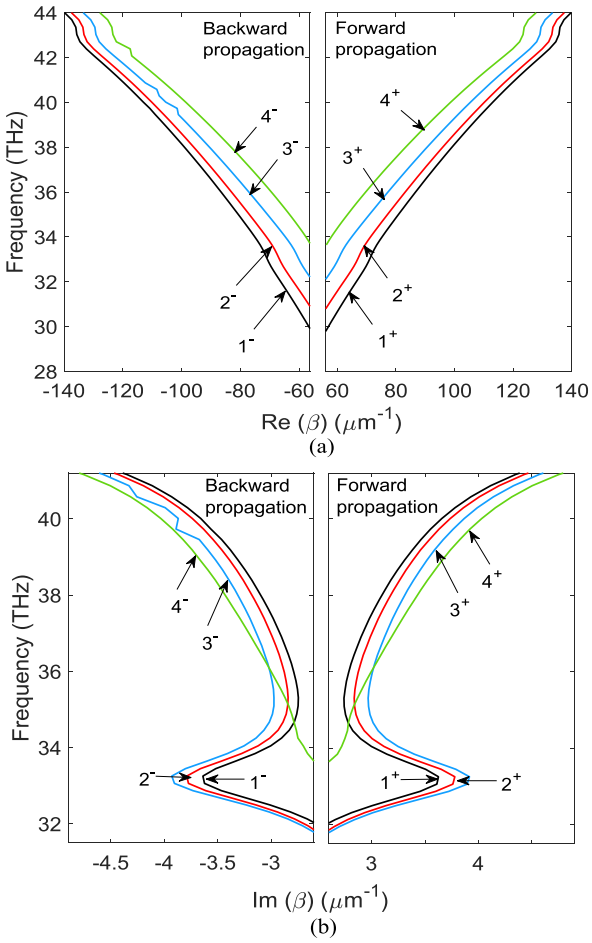

FIGURE 7. (a) Real part and (b) imaginary part of DLGMPW dispersion relation for the first 4 modes (the numbers 1,2,3,4 correspond to the modes order). Forward and backward propagation of SMPs are specified with + and – sign, respectively.

Moreover, at higher magnetic flux density, about B =5 T, Landau levels are separated more, which leads to sharp oscillation behavior (see Region1 in figure 5(c)). In this region, a small change in the wavelength, leads to a high deviation from single mode operation, due to the significant effective index change. Therefore, magneto-plasmon devices have a high sensitivity to the wavelength if they operate in such region. This phenomenon can be employed to realize ultra-high wavelength-sensitive sensors. Furthermore, in Region 2 of figure 5(c) another phenomenon occurs when a strong magnetic field is applied to DLGMPW. In this region, along cutline (A-D), from point A to B and from point C to D, we can see an ordinary behavior, that is, the number of supported mode decreases inversely with the wavelength. However, an extraordinary behavior is observed from point B to C, where a reverse change from the lower number of modes to the higher number of modes occurs by increasing wavelength. As it is shown, from point B to C, the number of supported modes increases from 2 to 4, which corresponds to a higher effective index of DLGMPW.

Fig. 6 shows the single mode and multimode operation regions of DLGMPW as a function of magnetic field and wavelength, for different values of chemical potential. By varying the magnetic field, the single mode operation region can be widely manipulated. Note that the magnetic-induced Landau level transitions, which are extremely sensitive to chemical potential, can profoundly change the mode operation region. As seen in Fig. 6(a), a lower chemical potential leads to a higher sensitivity to the magnetic field. The magnetic field effect decreases, as the chemical potential increases (see Fig. 6(c)). Therefore, the magnetic-induced tuning of the single mode and multimode region boundaries is more applicable in relatively low chemical potential. Moreover, as it is shown in Fig. 6(a), at a given wavelength, by varying the intensity of the magnetic field, we can change the number of guided modes and prevent some modes from propagating. Therefore, the number of modes is controlled by the external magnetic field and by such design we can obtain a mode switch.

The real and imaginary parts of DLGMPW dispersion relation for the first four modes are plotted in Figs. 7 (a) and (b) respectively using FEM, where the numbers 1,2,3,4 correspond to the modes order. As it is shown in Figs. 7 (a) and (b) an external magnetic field could break the mirror-symmetry of the waveguide dispersion relatively and possess nonreciprocal properties. Therefore, SMPs which are propagating in opposite directions, have slightly different propagation constants (β_{forward} & β_{backward}). This phenomenon can be employed to achieve ultra-compact nonreciprocal devices, such as isolators, circulators, nonreciprocal filters, and resonators.

IV. CONCLUSIONS

In this paper, we have proposed and studied a tunable dielectric-loaded magneto-plasmon waveguide. We have shown that graphene surface magneto-plasmons could be tuned via an external magnetic field, in addition to varying the graphene chemical potential. An analytical model based on EIM has been presented to investigate waveguide properties such as effective index, effective guide width, cutoff wavelength and the number of guided modes and then the results have been verified by finite element method. Analytical relations for effective mode index and effective thickness of waveguide have been derived through EIM. We have demonstrated that by applying an external magnetic field, an extraordinary behavior can be observed in DLGMPW. Without the magnetic field, the number of guided modes decreases inversely with respect to the wavelength. It can be observed that in the presence of a magnetic field, a reverse characteristic occurs in some regions, that is the number of guided modes increase with wavelength. In lower wavelengths, ultra-high This applies to papers in wavelength-sensitive regions have been made if the external magnetic field is sufficiently high. Moreover, it has been shown that the external magnetic field could control the number of guided modes and therefore, the proposed structure could be used as a mode switch device. Finally, we have shown that the waveguide becomes nonreciprocal in the presence of a magnetic field, which enables such structure to act as a plasmonic isolator and circulator.

ACKNOWLEDGMENT

M. Heidari thanks Mr. Rahman Sharaf, Mr. Babak Janjan and Mr. Mohammad Mahdi Mehrnegar for their help and fruitful discussions.

REFERENCES

[1] W. L. Barnes, A. Dereux, and T. W. Ebbesen, "Surface plasmon subwavelength optics," *Nature*, vol. 424, no. 6950, pp. 824–830, 2003.
[2] A. Ferreira, N. M. R. Peres, and A. H. C. Neto, "Confined magneto-optical waves in graphene," *Phys. Rev. B, Condens. Matter*, vol. 85, no. 20, 2012, Art. no. 205426.
[3] D. K. Gramotnev and S. I. Bozhevolnyi, "Plasmonics beyond the diffraction limit," *Nature Photon.*, vol. 4, no. 2, pp. 83–91, 2010.
[4] T. W. Ebbesen, C. Genet, and S. I. Bozhevolnyi, "Surface-plasmon circuitry," *Phys. Today*, vol. 61, no. 5, pp. 44–50, May 2008.
[5] E. Ozbay, "Plasmonics: Merging photonics and electronics at nanoscale dimensions," *Science*, vol. 311, pp. 189–193, Jan. 2006.
[6] K. F. MacDonald and N. I. Zheludev, "Active plasmonics: Current status," *Laser Photon. Rev.*, vol. 4, no. 4, pp. 562–567, 2010.
[7] T. Nikolajsen, K. Leosson, and S. I. Bozhevolnyi, "Surface plasmon polariton based modulators and switches operating at telecom wavelengths," *Appl. Phys. Lett.*, vol. 85, no. 24, pp. 5833–5835, Dec. 2004.
[8] M. J. Dicken, L. A. Sweatlock, D. Pacifici, H. J. Lezec, K. Bhattacharya, and H. A. Atwater, "Electrooptic modulation in thin film barium titanate plasmonic interferometers," *Nano Lett.*, vol. 8, no. 11, pp. 4048–4052, 2008.
[9] J. J. Brion, R. F. Wallis, A. Hartstein, and E. Burstein, "Theory of surface magnetoplasmons in semiconductors," *Phys. Rev. Lett.*, vol. 28, no. 22, pp. 1455–1458, May 1972.
[10] D. Pile and F. Xia, "Graphene versus metal plasmons," *Nature Photon.*, vol. 7, p. 420, Apr. 2013.
[11] M. D. Goldflam *et al.*, "Tunable dual-band graphene-based infrared reflectance filter," *Opt. Express*, vol. 26, no. 7, p. 8532, 2018.
[12] F. D. Parmentier *et al.*, "Quantum Hall effect in epitaxial graphene with permanent magnets," *Sci. Rep.*, vol. 6, Dec. 2016, Art. no. 38393.
[13] X. Y. He, J. Tao, and B. Meng, "Analysis of graphene TE surface plasmons in the terahertz regime," *Nanotechnology*, vol. 24, no. 34, 2013, Art. no. 345203.
[14] L. Ju *et al.*, "Graphene plasmonics for tunable terahertz metamaterials," *Nature Nanotechnol.*, vol. 6, no. 10, pp. 630–634, Sep. 2011.
[15] B. Hu, Y. Zhang, and Q. J. Wang, "Surface magneto plasmons and their applications in the infrared frequencies," *Nanophotonics*, vol. 4, no. 1, pp. 383–396, 2015.
[16] B. Hu, J. Tao, Y. Zhang, and Q. J. Wang, "Magneto-plasmonics in graphene-dielectric sandwich," *Opt. Express*, vol. 22, no. 18, pp. 21727–21738, 2014.
[17] F. Liu, C. Qian, and Y. D. Chong, "Directional excitation of graphene surface plasmons," *Opt. Express*, vol. 23, no. 3, pp. 2383–2391, Feb. 2015.
[18] M. Jablan, M. Soljacic, and H. Buljan, "Plasmons in graphene: Fundamental properties and potential applications," *Proc. IEEE*, vol. 101, no. 7, pp. 1689–1704, Jul. 2013.
[19] Q. Du *et al.*, "Monolithic on-chip magneto-optical isolator with 3 dB insertion loss and 40 dB isolation ratio," *ACS Photon.*, vol. 5, no. 12, pp. 5010–5016, Dec. 2018.
[20] S. Bahadori-Haghighi, R. Ghayour, and M. H. Sheikhi, "Three-dimensional analysis of an ultrashort optical cross-bar switch based on a graphene plasmonic coupler," *J. Light. Technol.*, vol. 35, no. 11, pp. 2211–2217, Jun. 1, 2017.
[21] M. Tamagnone *et al.*, "Near optimal graphene terahertz non-reciprocal isolator," *Nature Commun.*, vol. 7, Apr. 2016, Art. no. 11216.
[22] X. Lin, Z. Wang, F. Gao, B. Zhang, and H. Chen, "Atomically thin nonreciprocal optical isolation," *Sci. Rep.*, vol. 4, Feb. 2014, Art. no. 4190.
[23] J. Q. Liu, S. Wu, Y. X. Zhou, M. D. He, and A. V. Zayats, "Giant faraday rotation in graphene metamolecules due to plasmonic coupling," *J. Light. Technol.*, vol. 36, no. 13, pp. 2606–2610, Jul. 1, 2018.

[24] C. J. Firby and A. Y. Elezzabi, "High-speed nonreciprocal magnetoplasmonic waveguide phase shifter," *Optica*, vol. 2, no. 7, pp. 598–606, 2015.
[25] G. Armelles, A. Cebollada, F. García, A. García-Martín, and N. De Sousa, "Far- and near-field broad-band magneto-optical functionalities using magnetoplasmonic nanorods," *ACS Photon.*, vol. 3, no. 12, pp. 2427–2433, 2016.
[26] B. J. H. Stadler and T. Mizumoto, "Integrated magneto-optical materials and isolators: A review," *IEEE Photon. J.*, vol. 6, no. 1, Feb. 2014, Art. no. 0600215.
[27] H. Dötsch *et al.*, "Applications of magneto-optical waveguides in integrated optics: Review," *J. Opt. Soc. Amer. B*, vol. 22, no. 1, p. 240, 2005.
[28] D. Floess and H. Giessen, "Nonreciprocal hybrid magnetoplasmonics," *Rep. Prog. Phys.*, vol. 81, no. 11, Oct. 2018, Art. no. 116401.
[29] A. Pospischil *et al.*, "CMOS-compatible graphene photodetector covering all optical communication bands," *Nature Photon.*, vol. 7, p. 892, Sep. 2013.
[30] B. Zhu *et al.*, "Magnetically tunable non-reciprocal plasmons resonator based on graphene-coated nanowire," *Opt. Mater. Express*, vol. 5, no. 10, p. 2174, 2015.
[31] N. Chamanara, D. Sounas, and C. Caloz, "Non-reciprocal magnetoplasmon graphene coupler," *Opt. Express*, vol. 21, no. 9, pp. 11248–11256, 2013.
[32] W. Xu *et al.*, "Dielectric loaded graphene plasmon waveguide," *Opt. Express*, vol. 23, no. 4, p. 5147, 2015.
[33] D. L. Sounas and C. Caloz, "Edge surface modes in magnetically biased chemically doped graphene strips," *Appl. Phys. Lett.*, vol. 99, no. 23, 2011, Art. no. 231902.
[34] N. Chamanara, D. Sounas, T. Szkopek, and C. Caloz, "Terahertz magnetoplasmon energy concentration and splitting in graphene PN junctions," *Opt. Express*, vol. 21, no. 21, pp. 25356–25363, Oct. 2013.
[35] K. S. Chiang, "Dual effective-index method for the analysis of rectangular dielectric waveguides," *Appl. Opt.*, vol. 25, no. 13, pp. 2169–2174, 1986.
[36] H. Li *et al.*, "Analysis and design of photonic crystal fibers based on an improved effective-index method," *J. Lightw. Technol.*, vol. 25, no. 5, pp. 1224–1230, May 2007.
[37] G. W. Hanson, "Dyadic green's functions for an anisotropic, non-local model of biased graphene," *IEEE Trans. Antennas Propag.*, vol. 56, no. 3, pp. 747–757, Mar. 2008.
[38] V. P. Gusynin, S. G. Sharapov, and J. P. Carbotte, "Magneto-optical conductivity in graphene," *J. Phys., Condens. Matter*, vol. 19, no. 2, 2007, Art. no. 026222.
[39] I. V. Iorsh, I. V. Shadrivov, P. A. Belov, and Y. S. Kivshar, "Tunable hybrid surface waves supported by a graphene layer," *JETP Lett.*, vol. 97, no. 5, pp. 249–252, May 2013.
[40] H. Kogelnik and V. Ramaswamy, "Scaling rules for thin-film optical waveguides," *Appl. Opt.*, vol. 13, no. 8, pp. 1857–1862, 1974.
[41] H. Kogelnik and H. P. Weber, "Rays, stored energy, and power flow in dielectric waveguides," *J. Opt. Soc. Amer.*, vol. 64, no. 2, p. 174, 1974.
[42] A. Leblanc-Hotte, J.-S. Delisle, S. Lesage, and Y.-A. Peter, "The importance of single-mode behavior in silicon-on-insulator rib waveguides with very large cross section for resonant sensing applications," *IEEE J. Sel. Topics Quantum Electron.*, vol. 22, no. 6, pp. 241–248, Nov./Dec. 2016.

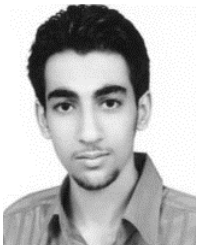

MOHSEN HEIDARI (S'08) received the B.S. and M.S. degrees in electrical engineering from the Department of Communication and Electronic Engineering, Shiraz University, Shiraz, Iran, in 2011 and 2013, respectively. He is currently pursuing the Ph.D. degree in electrical engineering with Tarbiat Modares University (TMU), Tehran, Iran. His current research interests include Graphene and 2D materials-based plasmonic and magneto-plasmonic, all-optical switches and modulators, plasmonic isolators, and nano-photonic devices.

VAHID AHMADI (M'86–SM'09) received the Ph.D. degree in electronic engineering from the Kyoto University, Japan, in 1994. He was the Head of the Semiconductor Department of Laser Research Centre, Tehran, from 1994 to 2006. He was the Head of the Electrical Engineering Department, TMU, from 2006 to 2008. He is currently a Professor in electronic engineering with Tarbiat Modares University (TMU), Tehran, Iran. His current research interests include nano-optoelectronic devices, nanophotonic, plasmonic, and biophotonic devices, nonlinear optics and slow light, optical quantum devices, tunable lasers and detectors, optical modulators, amplifiers and switches, micro-ring-based devices, photonic crystal and metamaterial-based devices, organic-based light sources and sensors, Perovskite-based solar cells and novel devices, photonic topological insulator-based devices, and graphene and 2D materials-based photonic devices. He is the member of the Founders-Board of Optics and Photonics Society of Iran; the editorial board of *International Journal of Information and Communication Technology Research* (IJICTR). He was the Technical and Scientific Chair of 13th Iranian Conf. on Optics and Photonics, in 2007, and the General Chair of the 16th Iranian Conference on Electrical Engineering (ICEE2008), in 2008. He is currently the Chair of the Optoelectronics and Photonics Research Group and the Head Nano-Optoelectronics Laboratory, TMU. He is also the Editor-in-Chief of *Modares Journal of Electrical Engineering*.